RESEARCH ARTICLE

HGT

Targeting Oncolytic Adenoviruses to Cancer Cells Using a Designed Ankyrin Repeat Protein Lipocalin-2 Fusion Protein

Sebastian Schellhorn,[1] Dominik Brücher,[2] Natascha A. Wolff,[3] Katrin Schröer,[1] Erwan Sallard,[1] Kemal Mese,[1] Wenli Zhang,[1] Eric Ehrke-Schulz,[1] Frank Thévenod,[3] Andreas Plückthun,[2] and Anja Ehrhardt[1,*]

[1]Virology and Microbiology, Center for Biomedical Education and Research (ZBAF), School of Medicine, Faculty of Health, Witten/Herdecke University, Witten, Germany; [2]Department of Biochemistry, University of Zurich, Zurich, Switzerland; [3]Institute of Physiology, Pathophysiology, and Toxicology, Center for Biomedical Training and Research (ZBAF), Witten/Herdecke University, Witten, Germany.

Oncolytic viruses are a promising technology to attack cancer cells and to recruit immune cells to the tumor site. Since the Lipocalin-2 receptor (LCN2R) is expressed on most cancer cells, we used its ligand LCN2 to target oncolytic adenoviruses (Ads) to cancer cells. Therefore, we fused a Designed Ankyrin Repeat Protein (DARPin) adapter binding the knob of Ad type 5 (knob5) to LCN2 to retarget the virus toward LCN2R with the aim of analyzing the basic characteristics of this novel targeting approach. The adapter was tested *in vitro* with Chinese Hamster Ovary (CHO) cells stably expressing the LCN2R and on 20 cancer cell lines (CCLs) using an Ad5 vector encoding luciferase and green fluorescent protein. Luciferase assays with the LCN2 adapter (LA) showed 10-fold higher infection compared with blocking adapter (BA) in CHO cells expressing LCN2R and in cells not expressing the LCN2R. Most CCLs showed an increased viral uptake of LA-bound virus compared with BA-bound virus and for five CCLs viral uptake was comparable to unmodified Ad5. Flow cytometry and hexon immunostainings also revealed increased uptake of LA-bound Ads compared with BA-bound Ads in most tested CCLs. Virus spread was studied in 3D cell culture models and nine CCLs showed increased and earlier fluorescence signals for LA-bound virus compared with BA-bound virus. Mechanistically, we show that the LA increases viral uptake only in the absence of its ligand Enterobactin (Ent) and independently of iron. Altogether, we characterized a novel DARPin-based system resulting in enhanced uptake demonstrating potential for future oncolytic virotherapy.

Keywords: adenovirus, DARPin, virotherapy, adenoviral vector, cancer, Lipocalin-2

INTRODUCTION

Around 20% of all people develop cancer before they turn 75, and half of them—10 million in 2020—die from it.[1] Therefore, next to commonly used radiotherapy, chemotherapy, and surgery, improved therapy options are urgently needed. Immunotherapy is an emerging therapy field, including numerous different approaches. Promising examples are checkpoint inhibitors (*i.e.* Pembrolizumab, Ateolizumab, Ipilimumab), chimeric antigen receptor T-cell therapy (*i.e.* Tisagenlecleucel, Axicabtagene ciloleucel), cytokines (*i.e.* Interleukin-2, Interferon-α), immunomodulators (*i.e.* Thalidomide, Lenalidomide, Pomalidomide), monoclonal antibodies (*i.e.* Brentuximab, Bevacizumab) or cancer vaccines (*i.e.* Sipuleucel-T, Talimogene laherparepvec [T-VEC]).[2–4]

T-VEC (Imlygic) was the first U.S. Food and Drug Administration (FDA)-approved oncolytic virus immunotherapy to treat cancer and consists of a herpes virus that

*Correspondence: Dr. Anja Ehrhardt, Virology and Microbiology, Center for Biomedical Education and Research (ZBAF), School of Medicine, Faculty of Health Witten/Herdecke University, Witten 58453, Germany. E-mail: anja.ehrhardt@uni-wh.de

DOI: 10.1089/hum.2022.215

predominantly infects cancer cells and expresses the immune-stimulating GM-CSF protein.[5] Currently different oncolytic virus platforms are being evaluated in clinical trials, among them are *Herpes simplex virus, measles virus, Newcastle Disease virus, picornavirus, reovirus, vaccinia virus, vesicular stomatitis virus, poxvirus, Seneca Valley virus, polio virus, coxsackievirus, parvovirus, retrovirus, alphavirus* and *adenovirus* (Ad).[6–9] Ads express 12 structural proteins, including the penton base (PB), protein IX, the hexon, and the trimeric fiber protein containing the C-terminal knob domain that mediates cell attachment.[10,11] Depending on the serotype, it can interact with several cell surface molecules such as the Coxsackie and Adenovirus Receptor (CAR),[10,12] CD46,[13] Desmoglein 2 (DSG-2),[14] GD1a,[15] and sialic acid residues.[16,17] After first contact with those molecules, Ads bind to integrins $\alpha_V\beta_3$ and $\alpha_V\beta_5$ through arginine–glycine–aspartic acid (RGD) motifs within their PB, which promotes virus internalization.[18,19]

Most viruses lack a natural tropism for tumor cells[20] and therefore there is a need for replication-competent viruses to be modified to specifically bind to and infect cancer cells. For the use in oncolytic therapies the replication itself can also be made preferential to cancer cells. Popular approaches include the modification of surface-exposed viral components or the use of bispecific adapters.[20] Such bispecific adapters usually contain at least two domains, one binding to the virion and one binding to an epitope of interest, leading to indirect interaction of the virus with the tumor cell.[20]

In our approach, we used the Lipocalin-2 receptor (LCN2R, Slc22A17, 24p3R) as cellular target, because of its expression on numerous cancer cells.[21–23] It interacts specifically with LCN2.[24,25] LCN2 is a 198 amino acid long secreted glycoprotein and is also expressed in many malignant tumors.[26] It participates in the antibacterial defense, by binding to bacterial siderophores like Enterobactin (Ent) that are loaded with iron (Fe). This ferric siderophore-complex-bound state is referred to as Holo-LCN2, whereas its unbound state is called Apo-LCN2.[27,28] Apo-LCN2 was shown to preferentially interact with the N-terminal domain of the LCN2R.[29]

Therefore, we designed and produced an LCN2 adapter (LA) molecule, consisting of a Designed Ankyrin Repeat Protein (DARPin) binding to the knob region of Ad5, a trimerization domain (SHP) and LCN2 (Fig. 1A). The SHP forms extremely stable trimers and thereby the symmetry of the trimeric knob is exploited and the adapter binds as a chelate.[30]

DARPins were first generated by the Plückthun laboratory[31–33] as alternatives for monoclonal antibodies that overcome certain limitations of the immunoglobulins like cost-intensive manufacturing, lower stability at harsh conditions (*e.g.*, high temperature), limited epitope coverage, and their tendency to aggregate especially when fused to additional domains as is the case in our work.[34]

In the present work, we tested if the LA can facilitate viral uptake of Ad5 into Chinese Hamster Ovary (CHO) model cell lines and into various cancer cell lines (CCLs) through luciferase assays, flow cytometry, hexon staining, and spheroid assays. The core aim of this study was to analyze the functionality and basic characteristics of this novel approach. In brief, we found that the LA increased virus uptake into various CCLs, but only in its Ent-free Apo-LA state. Altogether, we introduce a novel targeting approach and although this approach needs further analyses, we believe that there is high potential for future tumor treatment options.

MATERIALS AND METHODS

Cell culture

CHO K1 cells and CHO cells stably expressing LCN2R (CHO LCN2R) as well as heparan sulfate proteoglycan (HSPG)-deficient cell lines, CHO 745 and CHO 606, were cultivated in Dulbecco's modified Eagle's medium (DMEM, Pan-Biotech) with 10% fetal bovine serum (FBS), 1% penicillin–streptomycin (P/S), and 1% nonessential amino acids. CaCo-2 cells were cultivated in DMEM with 20% FBS and 1% P/S. Ca Ski cells were cultivated in RPMI 1640 Medium with 10% FBS and 1% P/S. HN cells, HNC cells, SCC cells, and HCT-116 cells were cultivated in MEM with 10% FBS and 1% P/S. HEK 293 cells, HeLa cells, SiHa cells, Hs578T cells, PLC/PRF/5 cells, MDA-MB-231 cells, MCF-7 cells, Hep-G2 cells, Hep-3B cells, SK-Hep-1 cells, SK-BR-3 cells, Huh-7 cells, and SK-OV-3 cells, were cultivated in DMEM with 10% FBS and 1% P/S. The cultivation was carried out in cell culture incubators running at a temperature of 37°C and a CO_2 level of 5%.

Viruses

Throughout the study, Ad5-GLN was explored, which was described in our previous work.[35] This replication-competent adenovirus type 5-based vector with an unmodified E1 transcription unit contains the GLN reporter cassette in the deleted E3 region, expressing TurboGFP, NanoLuc luciferase, and the selection marker kanamycin/neomycin.

Generation of a CHO cell model stably expressing the LCN2R

We first subcloned the *Rattus norwegicus* LCN2R/24p3R cDNA obtained from imaGenes into a pcDNA3.1 plasmid[25] and then transferred it into a pIRESneo3 expression plasmid (Clontech). This plasmid was then linearized with the *NruI* restriction enzyme, purified, and subsequently transfected into CHO K1 cells using the Promega FuGENE® 6 Transfection Kit. To select the cells for stable LCN2R expression, G418 (final concentration = 0.5 mg/mL) was added 24 h post-transfection. Afterward, single cell clones were selected by limited dilution, and followed by isolation of the resulting colonies. Note that G418 selection was maintained during the

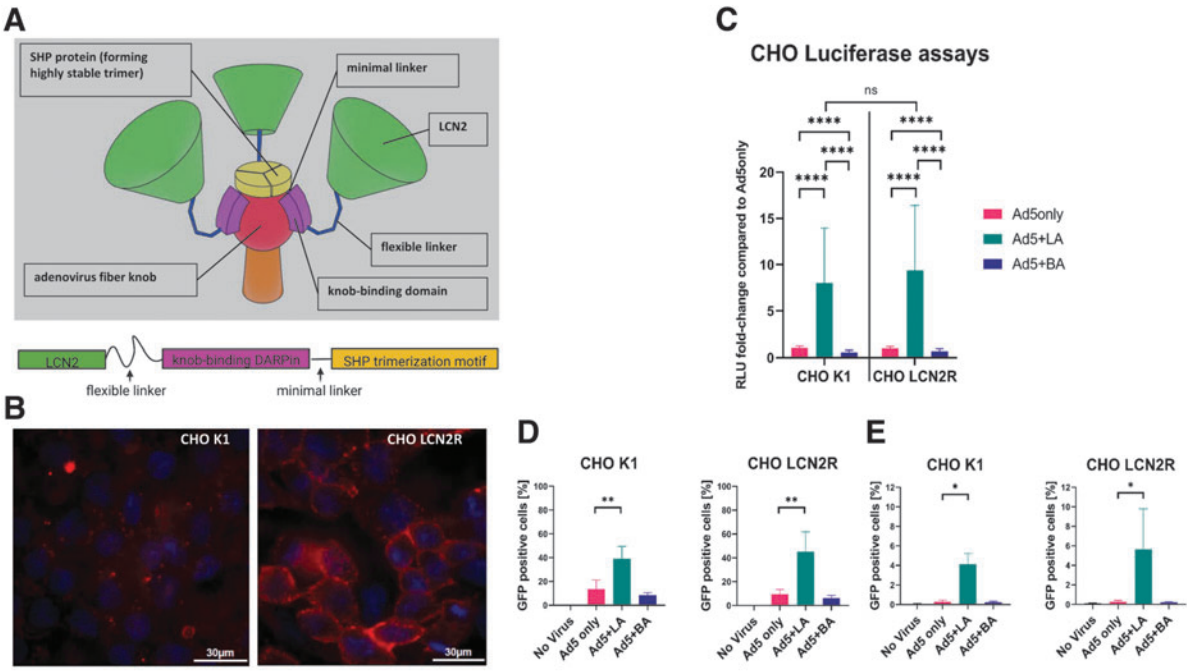

Figure 1. The LA increases viral uptake in a CHO cell model. **(A)** Schematic illustrations of the generated LCN2 DARPin fusion protein adapter (LA) containing the LCN2 (green) fused to the knob-binding DARPin (pink) through a flexible linker and the trimerization motif (yellow) that allows formation of the trimeric adapter molecule fused to the knob-binding DARPin through a short minimal linker. This DARPin is based on the DARPin described by Dreier et al.[30] The rendering of a 3D model adapter was generated with Blender and the illustration was created with BioRender.com. **(B)** The surface immunostaining of LCN2R for the CHO K1 untransfected control cells showed only a diffuse background signal compared with the clearly membrane-localized signal of the stably transfected CHO LCN2R cells. The cells were stained with an anti-LCN2R antibody and a nuclear counterstain. **(C)** Luciferase assay results 24 h postinfection (1000 vpc) of CHO K1 cells (no LCN2R expression) and CHO LCN2R-expressing cells. A nearly 10-fold increase of RLU for Ad5 incubated with LA compared with Ad5 alone (data normalized to Ad5only) was measured, while Ad5 incubated with the BA revealed a decrease in RLU. No differences between CHO K1 and LCN2R cell lines were detected (Mann–Whitney *U* test; $N=7$; ****p-value <0.0001). **(D)** Flow cytometry results 24 h postinfection (2000 vpc) of CHO K1 cells and CHO LCN2R-expressing cells show an increase in GFP-positive cells for Ad5 incubated with LA compared with Ad5 alone, whereas Ad5 incubated with BA shows a decrease (Mann–Whitney *U* test; $N=7$; *p-value <0.0332; **p-value <0.0021). **(E)** Hexon immunostaining flow cytometry results 3 h postinfection (2000 vpc) of CHO K1 cells and CHO LCN2R-expressing cells also show an increase in GFP-positive cells for Ad5 incubated with LA compared with Ad5 alone and incubated with BA (Mann–Whitney *U* test; $N=4$; *p-value <0.0332). BA, blocking adapter; CHO, Chinese Hamster Ovary; DARPin, Designed Ankyrin Repeat Protein; GFP, green fluorescent protein; LA, LCN2 adapter; LCN2R, Lipocalin-2 receptor; RLU, relative light unit.

complete selection procedure. Expression of the LCN2R in the CHO model was analyzed on the protein level through immunoblot (Supplementary Fig. S2) and surface immunostaining (Fig. 1B).

Surface immunostaining

To confirm LCN2R surface expression on stably transfected CHO cells, we performed a surface immunostaining. A total of 1×10^4 CHO K1 cells—serving as negative control—and CHO LCN2R cells were seeded onto glass coverslips. First, the cells were blocked for 1 h at 4°C in 1% BSA in Ca^{2+}/Mg^{2+} PBS. Next, the primary anti-LCN2R antibody (rabbit-anti-24p3R-NT #1095; 5 μg/mL; ImmunoGlobe)[25] was diluted in 1% BSA in Ca^{2+}/Mg^{2+} PBS and added to the cells. After incubation at 4°C for 2 h, the secondary antibody (Cy3-anti-rabbit; 1:600; Jackson ImmunoResearch Laboratories) was also diluted in 1% BSA in Ca^{2+}/Mg^{2+} PBS and added to the cells. After incubation at 4°C for 1 h, cells were fixed for 30 min at RT using 4% PFA in PBS.

The final step was a nuclear counter stain by incubating the cells with 0.8 μg/mL 2′-(4-ethoxyphenyl)-5-(4-methyl-l-piperazinyl)-2,5′-bi-1H-benzimidazole, 3HCl (H-33342; Calbiochem) in PBS, before the coverslips were mounted onto glass slides with DAKO fluorescence mounting medium. Image acquisition and processing were carried out essentially as described previously.[36]

DARPin adapter production

The production of the control adapters, blocking adapter (BA) (E2_5) and EGFR-binding adapters (EA), has been described by Dreier et al.[30] and apart from the replacement of the retargeting DARPin with LCN2, the LA follows a similar structure. The LA construct gene consists of the following elements in 5′ to 3′ prime direction: human serum albumin leader sequence, FLAG tag, His tag, GS linker, 3C cleavage site, Lipocalin-2, flexible linker, Ad5-knob-DARPin, and a SHP trimerization domain.

The LA construct was then expressed in CHO-S cells, followed by dialysis of the supernatant against PBS. Afterward, IMAC purification was performed and another dialysis of the eluate against PBS was conducted. Detection and purification tags were removed by 3C protease cleavage followed by a final size exclusion chromatography (SEC) polishing step using a Superdex 200 column. A scheme of the produced LA can be seen in Fig. 1A and the analytical SEC analysis and SDS gel electrophoresis in Supplementary Fig. S1. Note that the molecular weight of LA is larger than expected from the sequence, which may be caused due to glycosylation.

Virus adapter incubation

Ad5-GLN was incubated in a 1:100 knob:adapter molar ratio with either the BA or the LA for at least 1 h at RT. Since each viral particle carries 12 knob regions, to which the DARPin adapters can bind, 1 viral particle was incubated with 1200 adapter molecules. Note that for these calculations the number of optical viral particles and not the infectious virus particles were considered.

Additionally, the effect of Holo-LA was evaluated by incubation with Fe^{3+}, from $FeCl_3$ dissolved in water, with Enterochelin/Enterobactin (Ent) using a stoichiometry of 1:1 for 1 h at RT. Afterward either Fe^{3+} only, Ent only, or the resulting Fe^{3+}–Ent complex were incubated with the adapter molecules at a 1:1 ratio for 1 h at RT. Finally, the resulting complexes were incubated with Ad5 as described above.

Luciferase assay

First, 1×10^4 cells per well were seeded in a 96-well plate and incubated for 24 h in a cell culture incubator. Afterward, the cells were infected with 1×10^3 viral particles per cell (vpc) and incubated for another 24 h in a cell culture incubator. Then the luciferase assay was performed according to the manufacturer's protocol (Nano-Glo® Luciferase Assay, Promega). Briefly, the luciferase buffer was mixed with the luciferase substrate at a ratio of 50:1. Afterward, 50 μL of medium was kept inside each well and 50 μL of the substrate mix was added. The luminescence was measured using a TECAN Infinite F Plex Plate Reader after the plates were incubated for 10 to 30 min in a cell culture incubator. Then, the content of each well was transferred to a 96-well luciferase plate (Thermo Fisher Scientific Nunc A/S).

Flow cytometry

A total of 5×10^4 or 1×10^5 cells were seeded in each well of a 48-well plate. After 24 h, cells were infected using 1×10^3 or 2×10^3 vpc of Ad5only, Ad5+LA, and Ad5+BA, whereas uninfected cells served as negative control. Twenty-four hours after infection, cells were harvested by discarding the medium, carefully washing with Dulbecco's phosphate-buffered saline (DPBS, PanBiotech) and adding trypsin until all cells were detached. After either DMEM or DPBS containing 10% FBS was added to inhibit trypsin activity, cells were transferred to a V-shaped 96-well plate and centrifuged at 500 *g* for 5 min at RT. Then the supernatant was discarded and cells were washed with DPBS, followed by another centrifugation.

This time cells were fixed using 100 μL 2% formalin per well and incubated for 15 min at RT, followed by another centrifugation. After the supernatant was discarded, the cells were washed in DPBS, centrifuged, and the supernatant discarded once again. The final step consisted of resuspending the cells in 150 μL DPBS and transferring each well to a 96-well flow cytometry plate (Microtest plate 96 Well, Sarstedt).

The flow cytometry measurement was performed in a Beckman Coulter CytoFLEX flow cytometer counting 2×10^4 events. The FITC-A channel was used to measure green fluorescence indicating viral infection (due to the green fluorescent protein [GFP] expression from the GLN cassette).

Hexon-staining flow cytometry

A total of 5×10^4 cells were seeded in each well of a 48-well plate. After 24 h, cells were infected using 2×10^3 vpc of Ad5only, Ad5+LA, and Ad5+BA, whereas uninfected cells served as negative control. Three hours after infection, cells were harvested by discarding the medium, carefully washing with DPBS, and then trypsin was added until all cells were detached. After either DMEM or DPBS containing 10% FBS was added to inhibit trypsin activity, cells were transferred to a V-shaped 96-well plate and centrifuged at 500 *g* for 5 min at RT. Then the supernatant was discarded and cells were washed with DPBS, followed by another centrifugation. This time cells were fixed using either 100 μL of the Reagent A (Fix and Perm Zellpermeabilisierungskit, #GAS003; Thermo Fisher Scientific) or 100 μL 2% formalin per well and incubated for 15 min at RT, followed by another centrifugation. After the supernatant was discarded, the cells were washed in DPBS +10% FBS, centrifuged, and the supernatant discarded once again.

Then the cells were resuspended in a 100 μL mix of Reagent B (Fix and Perm Zellpermeabilisierungskit, #GAS003; Thermo Fisher Scientific) and 1:200 diluted primary anti-hexon antibody (Ms X Adenovirus, #MAB8052; Merck) and incubated overnight (ON) at 4°C. Once again, the cells were centrifuged and the supernatant discarded. Afterward, two washing steps consisting of resuspension in DPBS +10% FBS, centrifugation, and discarding of the supernatant were performed. The next step was an incubation in a 100 μL mix of Reagent B and 1:400 diluted fluorescent secondary antibody (Alexa Fluor™ 488 goat anti-mouse IgG1 (γ1); Invitrogen/Thermo Fisher Scientific) for 30 to 60 min in the dark. Again, two washing steps with DPBS were performed,

this time carefully protected from light. The final step consisted of resuspending the cells in 150 μL DPBS and transferring each well to a 96-well flow cytometry plate. The flow cytometry measurements were performed in a Beckman Coulter CytoFLEX flow cytometer counting 2×10^4 cells.

The cells were gated based on the FSC and SSC dot plot focusing on the presumably intact cell population. The FITC-A channel was used, to measure green fluorescence indicating viral infection. This workflow was based on Weaver and Kadan's comparative study.[37]

Cell Counting Kit-8 assay

A total of 1×10^4 cells were seeded in a 96-well plate (100 μL/well) and then incubated for 24 h in a cell culture incubator. Afterward, the cells were infected with 1000 vpc and incubated for another 24 h in a cell culture incubator. Finally, 10 μL of the Cell Counting Kit-8 (CCK-8) reagent (#ab228554; Abcam) was added to each well, the plate was incubated for 30 min and the absorbance at 450 nm was measured using a TECAN Infinite F Plex Plate Reader.

Spheroid assay

A total of 1×10^3 cells were seeded in a 96-well round bottom low-adherence plate (Greiner Bio-One, Microplate 96 well, PS, U-Bottom, clear, Cellstar® cell-repellent surface) and then incubated for 4 days in a cell culture incubator. On day 4, cells were infected using 1×10^6 viral particles of Ad5only, Ad5+LA, and Ad5+BA per well, whereas uninfected cells served as negative control. After that, cells were incubated for up to 14 days in a cell culture incubator and pictures were usually taken every 12 to 24 h either manually or automatically through the Incucyte® Live-Cell Imaging System.

GFP quantification

The quantification of GFP fluorescence for the automatic Incucyte spheroid assays was conducted with the inbuilt picture acquisition and analysis software, while the manual spheroid assays were analyzed with the ImageJ macro ''Flu-QoSI'' (Supplementary Fig. S3).

After picture acquisition with a fluorescence microscope and the LAS software, GFP fluorescence quantification was carried out, using the ImageJ Fiji application. The ''Flu-QoSI'' macro/plugin was written that was able to quantify the integrated density (mean gray value of an area of an 8-bit picture multiplied with its area) after splitting the color channels, focusing on the green channel, duplicating the image, using a fitting thresholding method, creating a mask and running a measurement on the green channel picture focusing only on the fluorescent area (so background was not an issue anymore). The quantification results were saved in a comma-separated values (CSV) file that could later be transferred to a Microsoft Excel document. The macro was able to batch-process subfolders, such that many pictures could be quantified automatically. For further details on the macro please refer to the supplemental material (Supplementary Fig. S3).

Statistical analysis

All experiments were conducted using three technical replicates. All luciferase experiments were repeated at least four times ($n \geq 4$). After normalizing the technical replicate values to the mean value of Ad5only for each experiment repetition, at least 12 normalized values per treatment could be compared, which enabled performance of unpaired, nonparametric Mann–Whitney U test. The CHO flow cytometry and hexon staining experiments were repeated four times ($n = 4$). The cancer cell flow cytometry analysis spheroid and oncolysis assays were conducted only once ($n = 1$).

RESULTS

Adapter increases viral uptake in CHO model cell lines

To create a cell culture model that differs only in the expression of the LCN2R, CHO K1 cells, which lack LCN2R expression, were stably transfected with a LCN2R expression plasmid. This cell line is referred to as CHO LCN2R.

Expression of the LCN2R was detected in CHO LCN2R cells and was absent in CHO K1 cells as demonstrated by immunoblot analysis (Supplementary Fig. S2) and surface immunostaining (Fig. 1B). In parallel, the 60 kDa LCN2R and a smaller 30 kDa isoform were observed for most CCLs in immunoblot analysis.

To bind to the LCN2R on the target cells, we generated the LA containing the LCN2 fused to the knob-binding domain and the trimerization domain (Fig. 1A). As a control, we also generated a BA, which binds to the knob and blocks its interaction site with CAR but is fused to a non-binding DARPin instead of LCN2. To establish if the generated adapter molecules incubated with Ad5 had an effect on its transduction properties, different adapter-to-knob ratios ranging from 1:10 to 1:10000 were tested. Performed luciferase assays showed an increase in relative light units (RLUs) for CHO K1 and CHO LCN2R cells after infection with Ad5+LA, compared with Ad5+BA or naked virus (termed Ad5only). This was possible because of the GLN cassette (encoding **G**FP, **l**uciferase, and **n**eomycin) present in our Ad5 vector inducing luciferase expression in transduced cells, which could then be measured 24 h postinfection.

For Ad5+LA, the RLU increasing effect was the highest with an adapter-to-knob ratio of 1:100, whereas for Ad5+BA, the same ratio showed the lowest RLU values (Supplementary Fig. S5). At very high molar excess, the adapter may bind both on the virus and on cells and thereby compete with virus uptake. Therefore, for all following experiments, we chose to use this ratio of one Ad5-knob to 100 LAs corresponding to one Ad5 virion

Table 1. *List of all cancer cell lines used in our experiments and results of luciferase assays, flow cytometry, spheroid assays, and oncolysis assays*

		Transduction Capability						*Oncolytic Effect*	
		Luciferase		*Flow Cytometry*		*Spheroid*		*CCK-8+C.V.*	
Cell Lines		*Ad5+LA*	*Ad5+BA*	*Ad5+LA*	*Ad5+BA*	*Ad5+LA*	*Ad5+BA*	*Ad5+LA*	*Ad5+BA*
Lung CCLs (epithelial)	A549			-	—	-	o		
Breast CCLs (epithelial)	SK-BR-3	+	-	-	—	o	o		
	MDA-MB-231	-	—	-	—			O	o
	MCF-7	o	-	O	-	o	-	O	-
	Hs578T	+	-	-	—	o	-	O	-
Cervical CCLs (epithelial)	SiHa	+	-			-	—	O	o
	HeLa	+		-	—	+	-	O	o
	Ca Ski	-	—	-	—			O	o
Ovarian CCL (epithelial)	SK-OV-3	+	o			o	o	O	o
	Caco-2	-	—			o	-	O	-
	HCT 116	o	+			o	-	O	o
Head and neck CCLs (epithelial)	HN-1497 (HN)	+	-			o	o		
	93VU147T (HNC)	o	-	-	—	o	-	O	o
	UPCI SCC 090 (SCC)	-	—			o	-		
Hepatic CCLs (epithelial)	Hep3B	+	-			o	o	O	o
	HepG2 (epithelial-like)	o	-	O	-	o	o		
	SK-Hep-1	+	-	O	-	o	o	O	o
	Huh-7	+	-			o	o	O	-
	PLC/PRF/5	+	o	O	-	o	-	O	-
	HepaRG	o	-	-	—	o	o	O	-
Ad5 transfected human embryonic kidney cells (epithelial)	HEK 293	+	++	O	-	o	o	O	-

The "+" indicates higher, the "o" equal and the "–" less transduction/oncolytic effect compared with Ad5only. Strong green fields indicate a significantly higher mean value compared with Ad5only (confirmed by Mann–Whitney *U* test), while light green ones showed a not significantly—but still higher—mean value. Accordingly, red fields showed decreased effects. A measurable oncolytic effect in the oncolysis assays (CCK-8 and/or Crystal Violet) is emphasized by a light orange color.

BA, blocking adapter; CCK-8, Cell Counting Kit-8; CCLs, cancer cell lines; LA, LCN2 adapter.

incubated with 1200 LA molecules (1 virion contains 12 knobs). Using the measured RLU as an indicator for viral transduction efficiency, we conclude that the LA increases viral uptake of Ad5 into both CHO cell models, whereas the BA blocks viral uptake. Replicate measurements, summarized in Fig. 1C, confirmed this effect. These results suggest that the LCN2 domain may interact also with receptors other than LCN2R (see Discussion).

To confirm these results, we performed flow cytometry analysis of the GFP expression 24 h postinfection. Ad5+LA was able to transduce around 50% of cells in both CHO cell lines, against no more than 15% for Ad5only and no more than 10% for Ad5+BA (Fig. 1D).

Furthermore, we tested the adapter effect on the early stages of viral uptake. At 3 h postinfection, infected cells were quantified by intracellular staining of the hexon protein of virus particles. Although the percentage of hexon-positive cells was relatively low, a strong adapter effect was observed. Hardly any hexon-positive cells were detected for Ad5only and Ad5+BA, whereas Ad5+LA showed significantly higher values in both CHO cell lines (Fig. 1E). The hexon immunostaining experiments 3 h postinfection confirm the results of luciferase assays and GFP-expression quantification.

LA increases viral uptake compared with BA in CCLs

To identify tumor types that our adapter enables to target more efficiently, we screened 20 CCLs (Table 1) using the same protocols as above.

Starting with the luciferase assay data (Fig. 2, summarized in Table 1), we found that in most tested CCLs Ad5+LA leads to higher viral uptake compared with Ad5+BA. Note that the knob region that interacts with CAR is blocked by both adapters. In five cases (SK-OV-3, HeLa, PLC/PRF/5, HN, SK-Hep-1) the natural viral uptake of Ad5 with its unbound knob region significantly exceeded Ad5+LA.

To confirm these results, additional flow cytometry analysis was performed on the CCLs (Fig. 3, summarized in Table 1). Most CCLs showed a similar number or slightly fewer GFP-positive cells for Ad5+LA compared with Ad5only, whereas the Ad5+BA percentages were consistently low. Overall, the flow cytometry results were in concordance with the luciferase data, showing increased infectivity for Ad5+LA compared with Ad5+BA, while not significantly exceeding the levels of Ad5only.

To test our adapter in a more clinically relevant model, we performed experiments in three-dimensional CCL

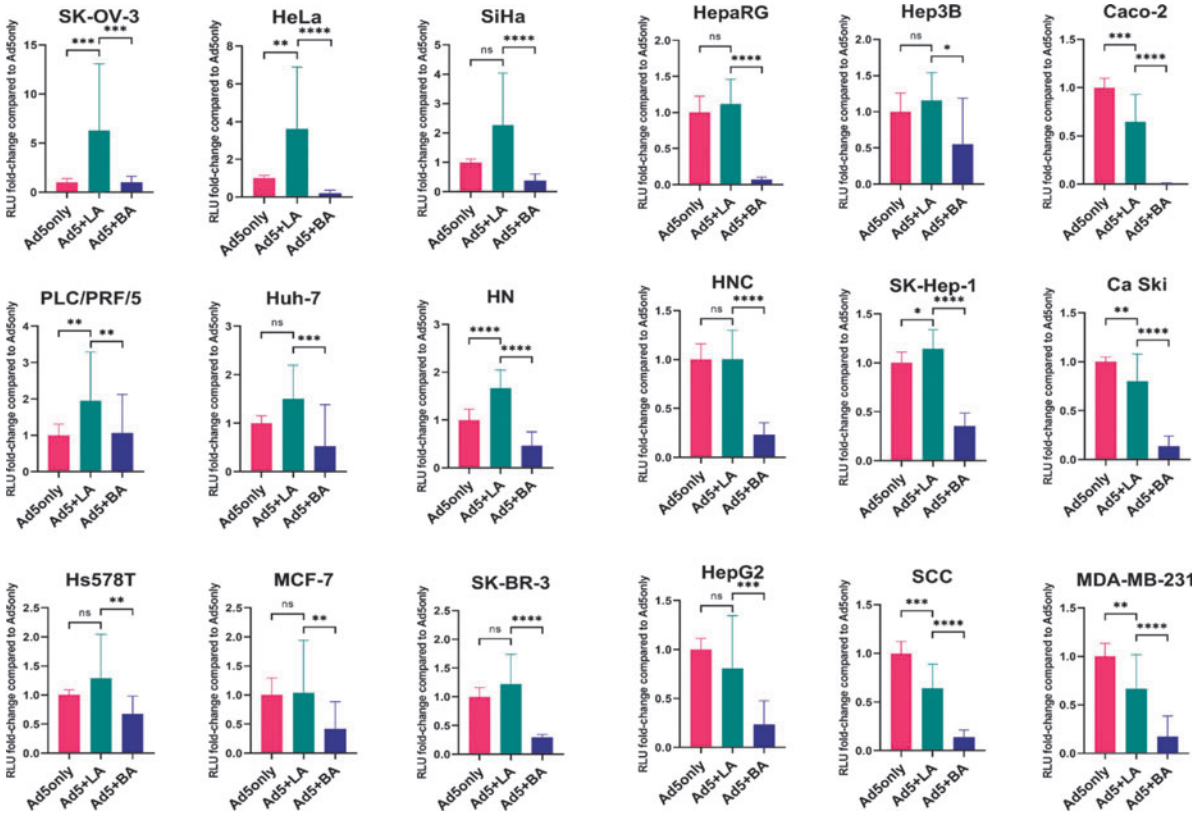

Figure 2. The LA increases viral uptake in CCLs. Luciferase assay results 24 h postinfection (1000 vpc) mostly show an increase of RLU for Ad5 incubated with LA compared with Ad5 alone, whereas Ad5 incubated with the BA shows a decrease (Mann–Whitney *U* test; $N \geq 12$; **p*-value <0.0332; ***p*-value <0.0021; ****p*-value <0.0002; *****p*-value <0.0001). CCLs, cancer cell lines.

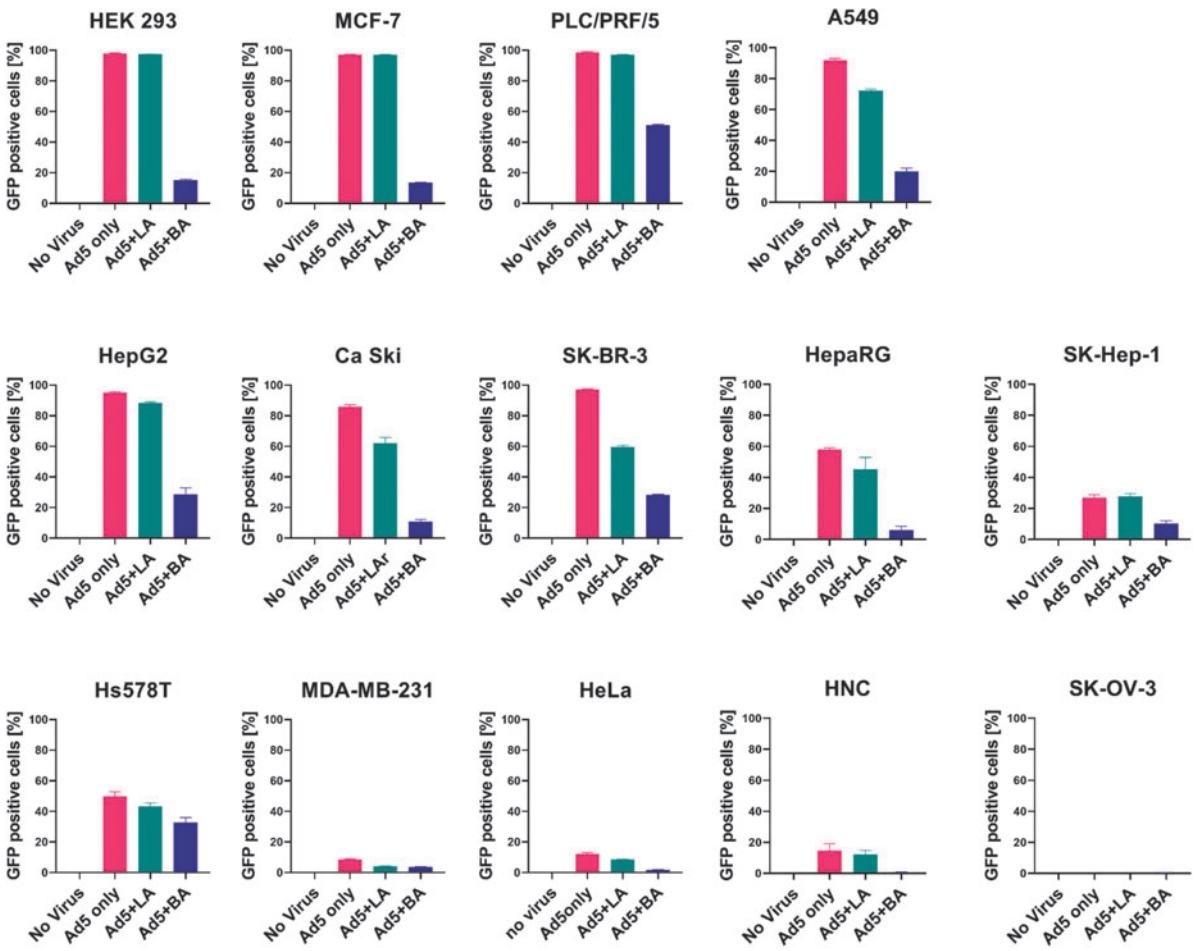

Figure 3. Ad5 incubated with the LA transduces CCLs similarly to Ad5 alone. Flow cytometry results 24 h postinfection (1000–2000 vpc) of various CCLs show an increase in GFP-positive cells for Ad5 incubated with LA compared with Ad5 incubated with the BA, but mostly similar levels compared with Ad5 alone ($N=1$; technical triplicates).

spheroid (mini-organoid) culture. After infection of the spheroid structures with our virus/adapter combinations, we tracked the spread of viral infection using a microscope and the Incucyte Live-Cell Imaging System to detect GFP fluorescence emitted by cells infected with Ad5. Representative videos of HeLa spheroid infection are shown in the Supplementary Videos S1–S4.

HeLa, SCC, HCT116, CaCo-2, HNC, Huh-7, HepG2, HEK-293, MCF-7, and Hs578T cell lines showed increased and earlier GFP fluorescence for Ad5+LA and Ad5only compared with Ad5+BA and a similar fluorescence signal when compared with each other (Fig. 4 and Supplementary Fig. S6). In HeLa, SCC, HEK293, MCF-7, and HCT116 cell lines, the Ad5+BA never reached the same fluorescence as Ad5only and Ad5+LA, whereas in CaCo-2, HNC, Huh-7, HepG2, and Hs578T cell lines, Ad5+BA reached a similar fluorescence level as Ad5only and Ad5+LA between 1 and 4 days later.

Ad5only and Ad5+LA showed comparable transduction in 2D and spheroids in HeLa, SCC, HN, HCT116, CaCo-2, HNC, Hep3B, and SK-Hep-1 cell lines, whereas Ad5+BA showed a delayed transduction profile. SK-OV-3, HepaRG, and Ca Ski cell lines proved to be quite resistant against viral infection.

LA increases oncolytic activity of Ad5 compared with BA

To determine if higher uptake of Ad5+LA also leads to an increased oncolytic effect on infected cells, we performed CCK-8 (Fig. 5) and Crystal Violet viability assays (Supplementary Fig. S7, both assays are summarized in Table 1). Considering that lower viability values may indicate a lytic effect induced by the viral infection, we detected noticeable differences between the CCLs. For HeLa, SiHa, MDA-MB-231, Ca Ski, SK-OV-3, and SK-Hep-1 cell lines either the dose was too low or the time span after infection was too short to show measurable oncolytic effects in the CCK-8 assay. Alternatively, these cell lines may not promote Ad5 proliferation. For the breast CCL MCF-7 as well as the hepatic CCLs HepaRG, PLC/PRF/5, Huh-7, and Hep3B, the colon CCLs Caco-2 and HCT116 and also the HEK293 cell line, we observed a

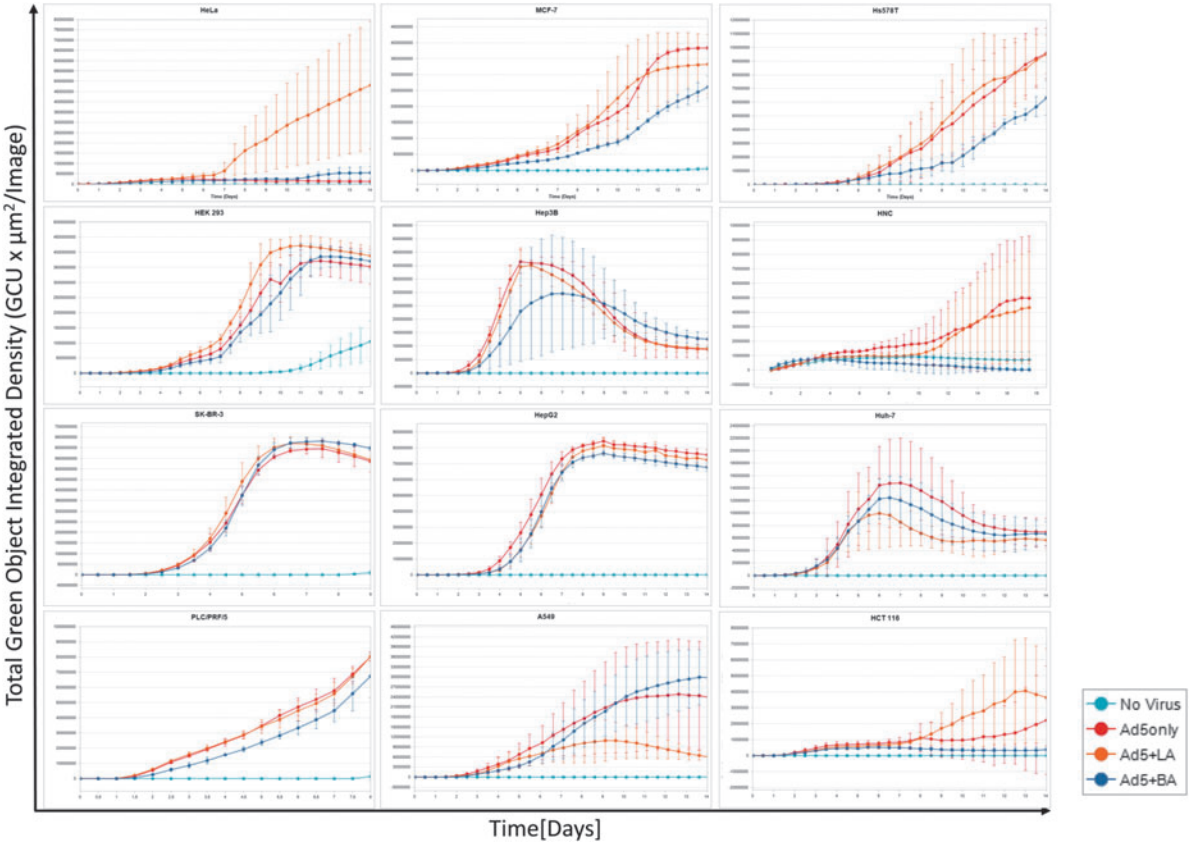

Figure 4. Ad5 incubated with the LA is able to infect spheroids of CCLs. For the Incucyte spheroid assay, 1×10^3 cells were seeded in a 96-well round *bottom* low adherence plate and spheroids were infected at day 4 (1000 vpc). Shown is the total *green* object integrated intensity (GCU $\times \mu m^2$/Image) of each spheroid image, which was monitored during the time course of the experiment. The integrated density includes information on both, the area and intensity of green fluorescence, and allows for depiction of both in one graph. Some CCLs show an earlier increase in GFP-expression for Ad5 incubated with the LA, when directly compared with Ad5 incubated with the BA. In most cell lines similar GFP intensity levels compared with Ad5 alone were observed ($N=1$; technical triplicates).

similar oncolytic effect for the Ad5–LA complex and for Ad5only. In contrast, HCT116, Huh-7, and Hep3B show similar cell death for Ad5 incubated with BA.

The Apo-LA but not the Ent-bound LA increases viral uptake in the CHO model cell lines

Since LCN2 acts as an iron transport molecule, through binding a siderophore (*i.e.*, Ent[28]) iron complex, it has two loading states. Holo-LCN2 describes the siderophore-iron-bound LCN2 and Apo-LCN2 the siderophore-iron-free LCN2. In the experiments described above we only used the Apo-state of the LA. Both forms are suggested to bind to the LCN2R,[24] therefore we decided to additionally include the Holo-LA in our assays. We performed flow cytometry analysis 24 h after infection of CHO K1 and CHO LCN2R cells with Ad5only, Ad5+LA, and Ad5+BA. We also included another targeting control adapter that contains a DARPin, specifically binding to the epidermal growth factor receptor (EGFR). This time the adapters were also incubated with Fe^{3+}, Ent, and FeEnt. The LA alone is considered the Apo-state, whereas the LA incubated with FeEnt is considered its Holo-state. We also included incubation of the LA with Fe^{3+} and Ent alone as controls.

Incubation with Fe^{3+}, Ent, or FeEnt had little effect on viral uptake of any of the control adapters, whereas the viral uptake effect seen for Ad5+LA was diminished back to Ad5only levels for Ent-bound LA and FeEnt-bound LA (Fig. 6). This suggests that Ent, bound or unbound to Fe^{3+}, blocks the mechanism that causes the increased viral uptake for Ad5+LA after binding to the LA. Since Fe^{3+}-bound LA (in the absence of Ent) maintained the uptake-increasing effect of LA and since Fe^{3+}-bound Ent (FeEnt) had the same diminishing effect as Ent alone, we conclude that the underlying mechanism is Fe^{3+} independent, and only dependent on the presence of Ent.

LA effect is not dependent on HSPGs

Since the increase in vector infectivity mediated by LA did not depend on LCN2R expression, we investigated whether other receptors were involved in the uptake of Ad5+LA. Because HSPGs were postulated to play a role in cellular uptake of some lipocalins,[38] we explored HSPG-deficient cells, such as the CHO 745 cell line lacking heparan sulfate chains[39] or the CHO 606 cell line having

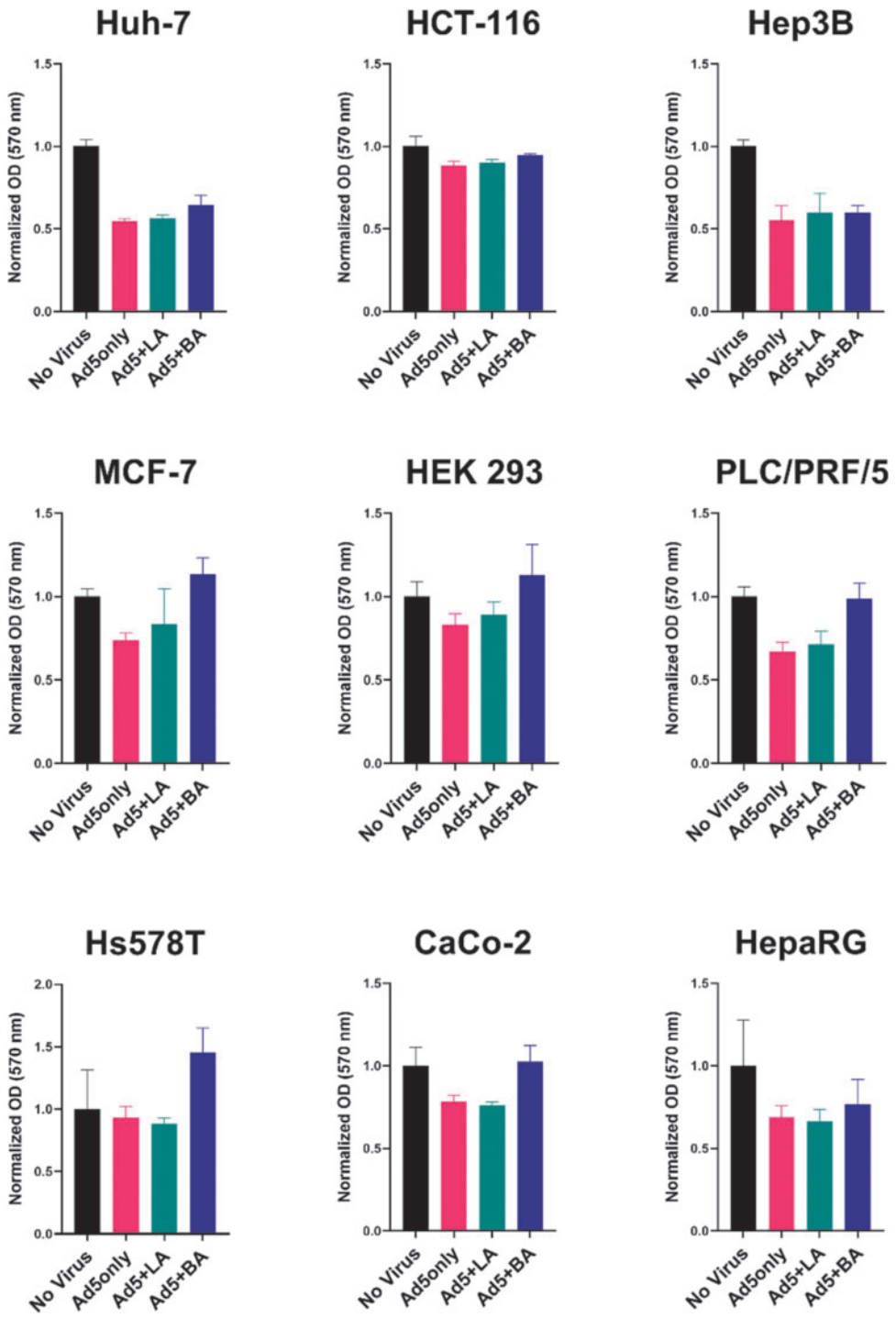

Figure 5. Ad5 incubated with the LA showed cancer cell killings. The CCK-8 cell viability assay was performed to analyze cancer cell killing efficiency. Various CCLs showed lower viability 5 days postinfection with Ad5 incubated with the LA compared with Ad5 incubated with the BA, but a similar viability as Ad5 alone ($N=1$; technical triplicates). CCK-8, Cell Counting Kit-8.

undersulfated HSPGs.[40] However, we still observed the viral uptake-increasing effect of the adapter (Supplementary Fig. S8). The LA-induced viral uptake increase was slightly but not significantly decreased in HSPG-deficient cell lines compared with CHO K1, excluding a major role of HSPGs in the uptake-increasing effect of the LA.

DISCUSSION

Our main hypothesis was that LA-bound virus would facilitate or even increase viral infection of cells through the interaction with the LCN2R on target cells. In our CHO cell models, the LA indeed significantly increased viral uptake of Ad5, which proves our main hypothesis in those

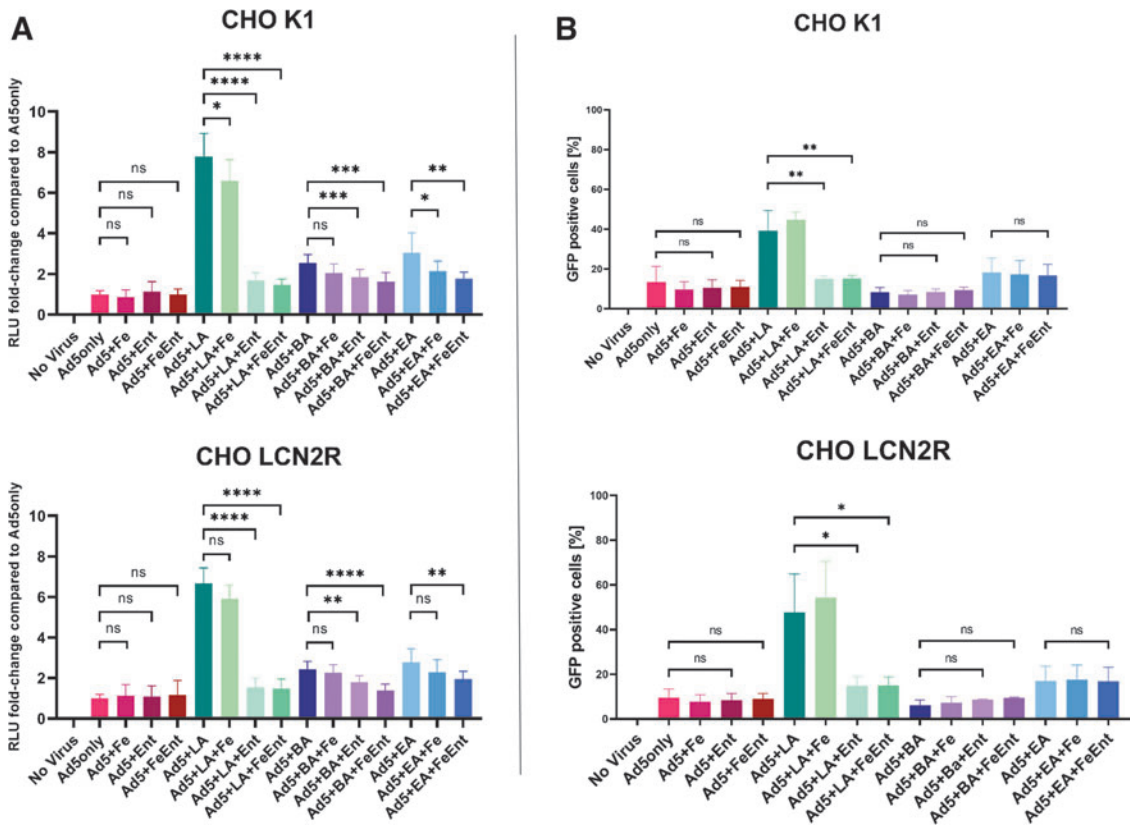

Figure 6. The Apo-LA but not the Ent-bound LA increases viral uptake in a CHO cell model. **(A)** Luciferase assays and **(B)** flow cytometry analysis were performed on CHO K1 and CHO LCN2R cells 24 h after infection with different complexes of Ad5/Ad5+LA/Ad5+BA/Ad5+EGFR-binding adapter (EA) with Fe^{3+}/Enterobactin (Ent)/FeEnt. Ad5+LA is considered the Apo-state and Ad5+LA+FeEnt is considered the Holo-state. The viral uptake increase after incubation of Ad5 with Apo-LA was greatly decreased by incubation with Ent- and FeEnt-bound LA instead. (Mann–Whitney *U* test; $N = 3$–21; **p*-value <0.0332; ***p*-value <0.0021; ****p*-value <0.0002; *****p*-value <0.0001).

cell models. However, our results also indicated a similar adapter effect for CHO cells with or without LCN2R expression, even though LCN2 has to be present on the adapter, since the BA does not have this effect.

This may indicate that the LA interaction with the LCN2R is not the only reason for the observed increase in viral uptake in this particular hamster-derived cell line. Therefore, a different mechanism or interaction partner might be causing this effect. Interactions of lipocalins with HSPGs were suggested by Habeler et al,[38] but since the LA-mediated transduction improvement was maintained in our luciferase experiments on HSPG-deficient CHO cell lines, HSPG may be excluded as the interaction partner. An alternative candidate cell receptor is megalin that has already been shown to bind both Apo- and Holo-LCN2 and both with equally high affinity ($K_d = \sim 60$ nM).[41]

While megalin might be a rational interaction partner candidate of the LA adapter, a screen of LA binding to different receptors should be conducted to identify and characterize the interaction partner in the future. To further characterize the novel adapter molecule, binding properties, including affinity, and avidity measurements should be performed. With respect to *in vivo* delivery of the adapter-decorated vectors, studying stability and potency of the adapter approach in the presence of mouse or human serum would add important information.

Investigation of Hs578T, PLC/PRF/5, HepaRG, SK-Hep-1, and HNC cells revealed an increased LA-mediated effect on viral uptake, compared with BA, using three different methods (luciferase assays, flow cytometry, and spheroid assays), which are encouraging findings for targeting hepatic cancer, head and neck cancer, and breast cancer. However, the most susceptible CCL in the spheroid assays was the HeLa cell line, which also showed a significant LA effect in luciferase assays compared with Ad5only. This suggests cervical cancer as a potential target for LA-enhanced virotherapy.

Since the oncolytic effect of replication-competent Ad5, yet carrying only reporter genes, was not sufficient to kill HeLa cells in our oncolysis assays and the increased uptake with our LA even induced rapid spheroid growth in the spheroid assays (Supplementary Videos S1–S4), our adapter should only be combined with armed viruses possessing increased cell lysis activity. The increased cell growth following viral infection has already been observed in independent experiments with different target cells and multiple

Ad serotypes by members of our group, but further experiments need to be conducted to shed light on this phenomenon.

Since a main function of LCN2 is suggested to be the antibacterial defense by capturing bacterial siderophores carrying iron and transporting the resulting Holo–LCN2 complex inside host cells, we expected to also see an increased uptake of virus incubated with LA and FeEnt. However, in both the CHO K1 and CHO LCN2R cell models, we observed a complete ablation of virus uptake after incubation with FeEnt. Furthermore, even LA incubation with Ent alone diminished the increased viral uptake effect of the LA. This might be due to a potential new interactor on the cell surface having different binding properties than the LCN2R, in other words hinting at the LA interacting with a different molecule than LCN2R. We cannot exclude the possibility, however, that the fused and trimerized LCN2 in the LA has different uptake properties than LCN2.

In our immunoblot experiments, we were able to detect the longer version of the LCN2R (around 60 kDa) and the shorter isoform (around 30 kDa), similarly to previously published immunoblot data.[24] However, in the present study, the HeLa cells showed LCN2R expression as well, which contradicts Devireddy's immunoblot data.[24] This dissimilarity could be caused by differences in the HeLa cell line cultivation or the antibody used for detecting the LCN2R used in both studies. Our antibody (Anti-Slc22A17 rabbit polyclonal, #ABC846; Merck) was purified by affinity chromatography and its immunogen was a KLH-conjugated synthetic peptide corresponding to the C-terminus of human Slc22A17, and it was shown to detect Slc22A17 in rat kidney tissue. Devireddy et al. used a polyclonal rabbit α-24p3R antibody that was raised using a C-terminal 24p3R peptide (CDHVPLLATPNAL) as the immunogen and affinity purified on a peptide-coupled Sepharose column.

Besides oncolytic adenoviruses, other viruses such as herpesvirus or measles virus could be applied for retargeting and/or detargeting studies using DARPin molecules. A study exploring a DARPin-retargeted oncolytic measles virus, which resulted in effective oncolysis associated with an improved safety profile, has already been published.[42]

The advantage of a bispecific adapter approach is that it can alter the binding properties of every adenovirus it is bound to. Additionally, by binding to the knob of Ads, the natural receptor—CAR, in the case of Ad5 leading to a broad tropism—can be blocked and altered to a more specific target (here: cancer cells). Furthermore, internalization of the virus–Apo–LA complex might result in dissociation of virus and LA, which in its Apo-state could add an additional oncolytic mechanism by iron depletion leading to apoptosis of the tumor cells.[24,43]

On the other hand, one has to keep in mind that probably only the originally LA-carrying virions will benefit from the improved viral uptake properties that the adapter provides, since it is not genetically encoded in the virus genomes and therefore not produced together with progeny virus particles. This could be circumvented by coinfection with a virus expressing the LA, or engineering the oncolytic Ads to express the LA themselves, which was already performed for other adapters.[44] Alternatively, the Ad can be constructed to encode therapeutic payloads.[45–47]

In the present study, we aimed at increasing the uptake of LA-coated Ad5-based oncolytic viruses to treat tumors, because the LCN2R was shown to be expressed on various cancer cells. In this study, we show proof-of-principle experiments of this approach *in vitro* in established CCLs. However, it needs to be emphasized that the described results and findings presented also demonstrate that the analyzed targeting approach seems more complex. We introduce a novel design of a new tumor treatment, which may require further investigation.

In the future, our work would be of benefit to additionally analyze the efficacy of this approach in primary patient-derived tumor cells. Furthermore, next steps should explore antitumor properties of LA-decorated oncolytic Ads in respective xenograft mouse tumor models. Besides investigating the novel DARPin-LA molecule in different *in vitro* and *in vivo* tumor cell models, it is also of relevance to explore Ads that are specifically replicating in tumors by insertion of tumor-specific promoters. In the present study, we used a replication-competent Ad5 vector retaining the early transcription unit E1 but lacking E3, which was replaced by the reporter encoding the GLN transgenes. To further optimize the oncolytic efficacy, the Ad5 genome could be genetically modified by, for instance, transcriptional targeting based on inserting a tumor-specific promoter for E1 expression or by post-transcriptional silencing through microRNA technology. Moreover, the oncolytic adenovirus could be armed by inserting additional transgenes such as TNFα, GM-CSF, other cytokines, or antibodies displaying additional antitumor effects.[45–47]

ACKNOWLEDGMENTS

The authors would like to thank Daniel Diehl, Oskar Bunz, and Raphael Tsoukas for support in cloning the plasmid encoding the LCN2R as well as Maximiliane Finkbeiner and Christine Engeland for their help regarding the Incucyte live-cell imaging system.

AUTHORS' CONTRIBUTIONS

S.S. conceived the study and performed a majority of the experiments. D.B. and A.P. produced the DARPin LCN2-adapter. K.S. performed HSPG-related studies. E.S. supported statistical analyses. W.Z. and E.E.-S. provided essential material. N.A.W. and F.T. performed surface immunostaining. K.M. was involved in conceiving the study. All authors who wrote and edited the article have agreed to its submission and are responsible for its content.

AUTHOR DISCLOSURE

W.Z. and A.E. are mentioned as coinventors on a patent with the application no. PCT/EP2017/058306 relevant for used vectors Ad5-GLN. All other authors, except for A.P. and D.B. declare no conflicts of interest. A.P. is a co-founder and shareholder and D.B. is an employee and shareholder of Vector BioPharma AG who are commercializing the adenovirus adapter technology.

FUNDING INFORMATION

This study was in part funded by the DFG grant EH 192/5–3 (to A.E.), the Westermann-Westdorp Foundation (to A.E., and K.M.), and the BMBF 01DN16039 (to F.T.).

SUPPLEMENTARY MATERIAL

Supplementary Figure S1
Supplementary Figure S2
Supplementary Figure S3
Supplementary Figure S4
Supplementary Figure S5
Supplementary Figure S6
Supplementary Figure S7
Supplementary Figure S8
Supplementary Video SV1
Supplementary Video SV2
Supplementary Video SV3
Supplementary Video SV4

REFERENCES

1. Ferlay J, Colombet M, Soerjomataram I, et al. Cancer statistics for the year 2020: An overview. Int J Cancer 2021;149:778–789; doi: 10.1002/ijc.33588
2. Quach H, Ritchie D, Stewart AK, et al. Mechanism of action of immunomodulatory drugs (IMiDS) in multiple myeloma. Leukemia 2010;24(1):S.22–S.32; doi: 10.1038/leu.2009.236
3. Christofi T, Baritaki S, Falzone L, et al. Current perspectives in cancer immunotherapy. Cancers 2019;11(10); doi: 10.3390/cancers11101472
4. Filin IY, Solovyeva VV, Kitaeva KV, et al. Current trends in cancer immunotherapy. Biomed 2020; 8(12); doi: 10.3390/biomedicines8120621
5. Ferrucci PF, Pala L, Conforti F, et al. Talimogene Laherparepvec (T-VEC): An intralesional cancer immunotherapy for advanced melanoma. Cancers 2021;13:1383; doi: 10.3390/cancers13061383
6. Harrington K, Freeman DJ, Kelly B, et al. Optimizing oncolytic virotherapy in cancer treatment. Nat Rev Drug Discov 2019;18(9):S.689–S.706; doi: 10.1038/s41573-019-0029-0
7. Cook M, Chauhan A. Clinical application of oncolytic viruses: A systematic review. Int J Mol Sci 2020;21(20); doi: 10.3390/ijms21207505
8. Macedo N, Miller DM, Haq R, Kaufman HL. Clinical landscape of oncolytic virus research in 2020. J Immunother Cancer 2020;8(2); doi: 10.1136/jitc-2020-001486
9. Yun C-O, Hong J, Yoon A-R. Current clinical landscape of oncolytic viruses as novel cancer immunotherapeutic and recent preclinical advancements. Front Immunol 2022;13:S.953410; doi: 10.3389/fimmu.2022.953410
10. Bergelson JM, Cunningham JA, Droguett G, et al. Isolation of a common receptor for Coxsackie B viruses and adenoviruses 2 and 5. Science 1997;275: 1320–1323; doi: 10.1126/science.275.5304.1320
11. Nemerow G, Flint J. Lessons learned from adenovirus (1970-2019). FEBS Lett 2019;593:3395–3418; doi: 10.1002/1873-3468.13700
12. Tomko RP, Xu R, Philipson L. HCAR and MCAR: the human and mouse cellular receptors for subgroup C adenoviruses and group B coxsackieviruses. Proc Natl Acad Sci U S A 1997;94: 3352–3356; doi: 10.1073/pnas.94.7.3352
13. Gaggar A, Shayakhmetov DM, Lieber A. CD46 is a cellular receptor for group B adenoviruses. Nat Med 2003;9:1408–1412; doi: 10.1038/nm952
14. Wang H, Li Z-Y, Liu Y, et al. Desmoglein 2 is a receptor for adenovirus serotypes 3, 7, 11 and 14. Nat Med 2011;17:96–104; doi: 10.1038/nm.2270
15. Nilsson EC, Storm RJ, Bauer J, et al. The GD1a glycan is a cellular receptor for adenoviruses causing epidemic keratoconjunctivitis. Nat Med 2011;17:105–109; doi: 10.1038/nm.2267
16. Arnberg N, Edlund K, Kidd AH, et al. Adenovirus type 37 uses sialic acid as a cellular receptor. J Virol 2000;74:42–48; doi: 10.1128/JVI.74.1.42–48.2000
17. Burmeister WP, Guilligay D, Cusack S, et al. Crystal structure of species D adenovirus fiber knobs and their sialic acid binding sites. J Virol 2004;78:7727–7736; doi: 10.1128/JVI.78.14.7727–7736.2004
18. Wickham TJ, Mathias P, Cheresh DA, et al. Integrins $\alpha v\beta 3$ and $\alpha v\beta 5$ promote adenovirus internalization but not virus attachment. Cell 1993; 73:309–319; doi: 10.1016/0092-8674(93)90231-E
19. Cheresh DA, Harper JR. Arg-Gly-Asp recognition by a cell adhesion receptor requires its 130-kDa alpha subunit. J Biol Chem 1987;262:1434–1437; doi: 10.1016/S0021-9258(19)75652-X
20. Verheije MH, Rottier PJM. Retargeting of viruses to generate oncolytic agents. Adv Virol 2012;2012: 798526; doi: 10.1155/2012/798526
21. Miyamoto T, Asaka R, Suzuki A, et al. Immunohistochemical detection of a specific receptor for lipocalin2 (solute carrier family 22 member 17, SLC22A17) and its prognostic significance in endometrial carcinoma. Exp Mol Pathol 2011;91: 563–568; doi: 10.1016/j.yexmp.2011.06.002
22. Wei J, Gao X, Qin Y, et al. An iron metabolism-related SLC22A17 for the prognostic value of gastric cancer. Onco Targets Ther 2020;13:12763–12775; doi: 10.2147/OTT.S287811
23. Chi Y, Remsik J, Kiseliovas V, et al. Cancer cells deploy lipocalin-2 to collect limiting iron in leptomeningeal metastasis. Science 2020;369:276–282; doi: 10.1126/science.aaz2193
24. Devireddy LR, Gazin C, Zhu X, et al. A cell-surface receptor for lipocalin 24p3 selectively mediates apoptosis and iron uptake. Cell 2005;123:1293–1305; doi: 10.1016/j.cell.2005.10.027
25. Langelueddecke C, Roussa E, Fenton RA, et al. Lipocalin-2 (24p3/neutrophil gelatinase-associated lipocalin (NGAL)) receptor is expressed in distal nephron and mediates protein endocytosis. J Biol Chem 2012;287:159–169; doi: 10.1074/jbc.M111.308296
26. Chakraborty S, Kaur S, Guha S, et al. The multifaceted roles of neutrophil gelatinase associated lipocalin (NGAL) in inflammation and cancer. Biochim Biophys Acta 2012;1826:129–169; doi: 10.1016/j.bbcan.2012.03.008
27. Yang J, Goetz D, Li J-Y, et al. An iron delivery pathway mediated by a lipocalin. Mol Cell 2002;10: 1045–1056; doi: 10.1016/S1097-2765(02)00710-4
28. Goetz DH, Holmes MA, Borregaard N, et al. The neutrophil lipocalin NGAL is a bacteriostatic agent that interferes with siderophore-mediated iron acquisition. Mol Cell 2002;10:1033–1043; doi: 10.1016/S1097-2765(02)00708-6
29. Cabedo Martinez A-I, Weinhäupl K, Lee W-K, et al. Biochemical and structural characterization of the interaction between the siderocalin NGAL/

LCN2 (neutrophil gelatinase-associated lipocalin/lipocalin 2) and the N-terminal domain of its endocytic receptor SLC22A17. J Biol Chem 2016; 291:2917–2930; doi: 10.1074/jbc.M115.685644

30. Dreier B, Honegger A, Hess C, et al. Development of a generic adenovirus delivery system based on structure-guided design of bispecific trimeric DARPin adapters. Proc Natl Acad Sci U S A 2013; 110:E869–E877; doi: 10.1073/pnas.1213653110

31. Binz H, Stumpp MT, Forrer P, et al. Designing repeat proteins: Well-expressed, soluble and stable proteins from combinatorial libraries of consensus ankyrin repeat proteins. J Mol Biol 2003; 332:489–503; doi: 10.1016/S0022-2836(03)00896-9.

32. Kohl A, Binz HK, Forrer P, et al. Designed to be stable: Crystal structure of a consensus ankyrin repeat protein. Proc Natl Acad Sci U S A 2003; 100:1700–1705; doi: 10.1073/pnas.0337680100

33. Forrer P, Binz HK, Stumpp MT, et al. Consensus design of repeat proteins. Chembiochem 2004;5: 183–189; doi: 10.1002/cbic.200300762

34. Binz HK, Amstutz P, Plückthun A. Engineering novel binding proteins from nonimmunoglobulin domains. Nat Biotechnol 2005;23:1257–1268; doi: 10.1038/nbt1127

35. Zhang W, Fu J, Liu J, et al. An engineered virus library as a resource for the spectrum-wide exploration of virus and vector diversity. Cell Rep 2017; 19:1698–1709; doi: 10.1016/j.celrep.2017.05.008

36. Abouhamed M, Gburek J, Liu W, et al. Divalent metal transporter 1 in the kidney proximal tubule is expressed in late endosomes/lysosomal membranes: Implications for renal handling of protein-metal complexes. Am J Physiol Renal Physiol 2006; 290:F1525–F1533; doi: 10.1152/ajprenal.00359.2005

37. Weaver LS, Kadan MJ. Evaluation of adenoviral vectors by flow cytometry. Methods 2000;21:297–312; doi: 10.1006/meth.2000.1010

38. Habeler M, Lindner HH, Redl B. A role of heparan sulphate proteoglycan in the cellular uptake of lipocalins ß-lactoglobulin and allergen Fel d 4. Biol Chem 2020;401:1081–1092; doi: 10.1515/hsz-2020-0132

39. Esko JD, Stewart TE, Taylor WH. Animal cell mutants defective in glycosaminoglycan biosynthesis. Proc Natl Acad Sci U S A 1985;82:3197–3201; doi: 10.1073/pnas.82.10.3197

40. Bame KJ, Esko JD. Undersulfated heparan sulfate in a Chinese Hamster Ovary cell mutant defective in heparan sulfate N-sulfotransferase. J Biol Chem 1989;264:8059–8065; doi: 10.1016/S0021-9258(18)83150-7

41. Hvidberg V, Jacobsen C, Strong RK, et al. The endocytic receptor megalin binds the iron transporting neutrophil-gelatinase-associated lipocalin with high affinity and mediates its cellular uptake. FEBS Lett 2005;579:773–777; doi: 10.1016/j.febslet.2004.12.031

42. Friedrich K, Hanauer JR, Prüfer S, et al. DARPin-targeting of measles virus: Unique bispecificity, effective oncolysis, and enhanced safety. Mol Ther 2013;21:849–859; doi: 10.1038/mt.2013.16

43. Devireddy LR, Teodoro JG, Richard FA, et al. Induction of apoptosis by a secreted lipocalin that is transcriptionally regulated by IL-3 deprivation. Science 2001;293:829–834; doi: 10.1126/science.1061075

44. van Beusechem VW, Mastenbroek DCJ, van den Doel PB, et al. Conditionally replicative adenovirus expressing a targeting adapter molecule exhibits enhanced oncolytic potency on CAR-deficient tumors. Gene Ther 2003;10:1982–1991; doi: 10.1038/sj.gt.3302103

45. Smith SN, Schubert R, Simic B, et al. The SHREAD gene therapy platform for paracrine delivery improves tumor localization and intratumoral effects of a clinical antibody. Proc Natl Acad Sci U S A 2021;118; doi: 10.1073/pnas.2017925118

46. Brücher D, Kirchhammer N, Smith SN, et al. iMATCH: an integrated modular assembly system for therapeutic combination high-capacity adenovirus gene therapy. Mol Ther Methods Clin Dev 2021; 20:572–586; doi: 10.1016/j.omtm.2021.01.002

47. Kirchhammer N, Trefny MP, Natoli M, et al. NK cells with tissue-resident traits shape response to immunotherapy by inducing adaptive antitumor immunity. Sci Transl Med 2022;14:eabm9043; doi: 10.1126/scitranslmed.abm9043

Received for publication November 11, 2022;

accepted after revision January 23, 2023.

Published online: February 18, 2023.